Editors' Suggestion

Surface-field-induced heliconical instability in the cholesteric phase of a mixture of a flexible dimer (CB7CB) and a rodlike molecule (8CB)

Patrick Oswald*

Univ Lyon, ENS de Lyon, Univ Claude Bernard, CNRS, Laboratoire de Physique, F-69342 Lyon, France

(Received 21 October 2021; accepted 1 December 2021; published 18 February 2022)

In 1968, de Gennes and Meyer independently predicted that a cholesteric phase can form a stable oblique helicoidal (or heliconical) structure provided that $K_3 < K_2$ where K_3 (K_2) is the bend (twist) constant. This structure usually develops under electric field when the material is of positive dielectric anisotropy and was observed for the first time in 2014 by Xiang *et al.* in a cholesteric phase made of a liquid crystal dimer material (CB7CB) in which K_3 is anomalously small. Following a recent theoretical prediction by Poy and Žumer, I show that confining a similar cholesteric phase between two glass plates treated for unidirectional anchoring can lead to a similar heliconical instability. In that case, the confinement induces a surface field that acts as an effective electric field E with $E \equiv 1/d$ where d is the sample thickness. The experiment was conducted in a mixture of CB7CB +50 wt% 8CB doped with a small amount of the chiral molecule R811. In addition, I show that this mixture presents an unexpected compensation point near the transition to the N_{TB} phase.

DOI: 10.1103/PhysRevE.105.024704

I. INTRODUCTION

By doping a nematic phase with a small amount of a chiral molecule, one obtains a cholesteric phase in which the director $\vec{n}$ rotates along a space direction called the helical axis [1]. In the structure at equilibrium, the director is perpendicular to the helical axis. If the bend elastic constant K_3 is smaller than the twist elastic constant K_2 and if the dielectric anisotropy $\varepsilon_a = \varepsilon_\parallel - \varepsilon_\perp$ of the liquid crystal is positive, it is possible to induce, by imposing an electric field E, a new director configuration in which the director follows an oblique helicoid. This result was independently shown by Meyer [2] and de Gennes [3] in 1968. The pitch P of this structure, also called the heliconical pitch, is inversely proportional to the field [2]:

$$P = \frac{2\pi}{E}\sqrt{\frac{K_3}{\varepsilon_0 \varepsilon_a}} \tag{1}$$

and is independent of the equilibrium pitch P_0 of the cholesteric phase.

This solution develops when the electric field is decreased below a critical field [2]

$$E_c = \frac{2\pi}{P_0}\frac{K_2}{\sqrt{\varepsilon_0 \varepsilon_a K_3}} \tag{2}$$

above which the cholesteric phase is unwound and disappears at fields lower than [4]

$$E_c^\star \approx E_c \frac{\kappa(2+\sqrt{2(1-\kappa)})}{1+\kappa}, \tag{3}$$

where $\kappa = K_3/K_2$.

This solution was observed for the first time by Xiang *et al.* [4] in the cholesteric phase of the bent flexible dimer CB7CB doped with the chiral molecule S811 (for a review on the physical properties of liquid crystals (LC) of bent-shaped molecules, see Ref. [5]) and was then intensively studied for its capabilities in producing Bragg and Raman-Nath diffraction and mirrorless lasing (for a review, see Ref. [6]).

In this paper, I show experimentally that a similar solution can be observed in a cholesteric phase confined between two plates treated for planar unidirectional anchoring. In this geometry, the confinement can be used to unwind the cholesteric phase and acts as an electric field. In that case, the equivalent electric field is a surface field, which is here simply the reciprocal of the sample thickness d. Indeed, it is well known that the cholesteric phase unwinds when $1/d > 4/P_0$ [1]. By analogy with the instability discovered by de Gennes and Meyer, one can thus wonder if a confined unwound cholesteric can become unstable with respect to a heliconical deformation when its bend constant K_3 is very small. This result was actually demonstrated by Poy and Žumer in a recent paper about the nonlinear optical response of a frustrated cholesteric phase [7]. The aim of this paper is to show experimentally that this instability does exist.

The plan of the paper is as follows. In Sec. II, I recall the theoretical results obtained by Poy and Žumer about the heliconical instability of the unwound solution in materials with low K_3 when the sample thickness is less than $P_0/4$. I then extend this analysis to the case of the π-twisted solution that is usually observed when $P_0/4 < d < 3P_0/4$ [1] and I show that a similar instability can develop. In Sec. III, I show experimentally that this instability does exist in both unwound and π-twisted cholesteric samples and I compare the experimental results with the theoretical predictions. Conclusions and perspectives are drawn in Sec. IV.

II. THEORETICAL PREDICTIONS

I consider a cholesteric sample sandwiched between two glass plates treated for strong planar unidirectional anchoring

*patrick.oswald@ens-lyon.fr

along the x axis. The z axis is taken perpendicular to the plates and d is the sample thickness. When $d < P_0/4$ it is well known that the cholesteric phase unwinds and adopts a planar nematic-like structure while a planar π-twisted solution develops when $P_0/4 < d < 3P_0/4$. In most of the liquid crystals, the bend constant K_3 is larger than the splay and twist constants K_1 and K_2 and these solutions are stable. The situation changes when K_3 is small as shown recently by Poy and Žumer [7] by analyzing the stability of the unwound solution. In Sec. II B, I recall their main results. I will then generalize the calculation to the case of the π-twisted solution.

A. Stability of the unwound solution

In their paper, Poy and Žumer analyze the determinant of the self-adjoint differential operator governing the linear response of the liquid crystal under the action of an external field. This method is very general but a bit complicated. The same result can be obtained by determining under which conditions a perturbation of the type $\vec{n} = \vec{n}_0/\|\overrightarrow{n_0}\|$ with

$$\vec{n}_0 = \begin{pmatrix} 1 \\ \delta n_y \sin\left(\frac{\pi z}{d}\right)\sin(qx) \\ \delta n_z \sin\left(\frac{\pi z}{d}\right)\sin(qx+\phi) \end{pmatrix} \tag{4}$$

becomes energetically favorable. Calculating the elastic free energy per unit surface area:

$$F = \frac{q}{2\pi}\int_0^{2\pi/q}\int_0^d f dx dz, \tag{5}$$

where

$$f = \frac{1}{2}K_1 \mathrm{div}(\vec{n})^2 + \frac{1}{2}K_2[\vec{n}.\vec{\mathrm{curl}}(\vec{n}) + q_0]^2 + \frac{1}{2}K_3[\vec{n}\times\vec{\mathrm{curl}}(\vec{n})]^2 \tag{6}$$

gives, to second order in deformation,

$$F = \tfrac{1}{2}dK_2q_0^2 + \tfrac{\pi^2K_2+d^2q^2K_3}{8d}\delta n_y^2 + \tfrac{\pi^2K_1+d^2q^2K_3}{8d}\delta n_z^2 + \tfrac{1}{2}K_2dqq_0\sin(\phi)\delta n_y\delta n_z. \tag{7}$$

The system becomes unstable when the discriminant Δ of this quadratic form in $(\delta n_y, \delta n_z)$:

$$\Delta = \tfrac{(\pi^2K_1+d^2q^2K_3)(\pi^2K_2+d^2q^2K_3)-4d^4q^2q_0^2K_2^2\sin(\phi)^2}{16d^2} \tag{8}$$

becomes negative. This imposes that $\phi = \pm\pi/2$ and that the equilibrium twist q_0 is larger (in absolute value) than some critical value [7]

$$q_{0c} = \frac{\pi}{d}\frac{\sqrt{K_3}(\sqrt{K_1}+\sqrt{K_2})}{2K_2}. \tag{9}$$

Equivalently, the ratio P_0/d must be smaller (in absolute value) than the ratio

$$\left(\frac{P_0}{d}\right)_{\max 1} = \frac{4K_2}{\sqrt{K_3}(\sqrt{K_1}+\sqrt{K_2})}. \tag{10}$$

This condition was already given in Ref. [7]. At the onset of instability, when $|q_0| = q_{0c}$ or $|P_0/d| = (P_0/d)_{\max 1}$, the discriminant vanishes for

$$|q| = q_{c1} = \frac{\pi}{d}\frac{(K_1K_2)^{1/4}}{\sqrt{K_3}}. \tag{11}$$

This defines the wavelength at the onset of instability:

$$\lambda_{c1} = 2\pi/q_{c1} = \frac{2\sqrt{K_3}}{(K_1K_2)^{1/4}}d. \tag{12}$$

This formula was also given in Ref. [7]. A remarkable point is that this wavelength is independent of the equilibrium twist of the cholesteric phase. Finally, the ratio $\delta n_y/\delta n_z$ can be calculated at the onset of instability. It is given by

$$\frac{\delta n_y}{\delta n_z} = -\mathrm{sign}(q_0)\left(\frac{K_1}{K_2}\right)^{1/4} \tag{13}$$

by choosing, without any loss of generality, $\phi = \pi/2$ and $q = q_{c1}$.

This formula (not given in Ref. [7]) shows that the director rotates in the midplane of the sample on a cone of axis parallel to the anchoring direction on the plates, proving that we are well dealing with a heliconical instability. This cone is axisymmetric if $K_1 = K_2$ and slightly flattened otherwise [with a flattening given by $(K_1/K_2)^{1/4}$]. As expected, the sense of rotation of the director on the cone is given by the sign of q_0.

Finally, note that when $|q_0| > q_{0c}$, there is a band of unstable wavelengths $[\lambda_{\min}, \lambda_{\max}]$. These two wavelengths are given by $\lambda_{\min} = 2\pi/q_{\max}$ and $\lambda_{\max} = 2\pi/q_{\min}$, where $q_{\max}$ and $q_{\min}$ are the solutions of equation $\Delta = 0$ with $\phi = \pm\pi/2$. A direct calculation gives:

$$\begin{cases} \lambda_{\min} = \dfrac{2\pi\sqrt{2}K_3\,d}{\sqrt{\mathcal{K}+\sqrt{\mathcal{K}^2-4\pi^4K_1K_2K_3^2}}} \\ \lambda_{\max} = \dfrac{2\pi\sqrt{2}K_3\,d}{\sqrt{\mathcal{K}-\sqrt{\mathcal{K}^2-4\pi^4K_1K_2K_3^2}}} \end{cases}, \tag{14}$$

where

$$\mathcal{K} = 4K_2^2d^2q_0^2 - \pi^2(K_1+K_2)K_3. \tag{15}$$

Of course, $\lambda_{\min} = \lambda_{\max} = \lambda_{c1}$ when $q_0 = q_{0c}$. Experimentally, the system will select a wavelength in the interval $[\lambda_{\min}, \lambda_{\max}]$. One could think that the most unstable wavelength is selected. It is possible to calculate this wavelength by calculating the principal curvatures of the potential at the origin. Above the onset of instability, one of them becomes negative and there is a wavelength for which it is minimal. This defines the most unstable wavelength. This calculation is straightforward but I have found that this wavelength is very different from the measured wavelength. For this reason, I will not detail this calculation here. This simply shows that only a full nonlinear analysis of the problem can give the measured wavelength. This is, however, beyond the scope of the present study.

In practice, this heliconical solution will be observable and stable with respect to the nucleation of the π-twisted solution only in samples of thickness $d < |P_0|/4$. This imposes that $4 < |P_0|/d < (P_0/d)_{\max}$. This is only possible in materials in

which the elastic constants satisfy the following condition:

$$g_1(K_1, K_2, K_3) := \sqrt{K_3}\frac{\sqrt{K_1}+\sqrt{K_2}}{K_2} < 1. \tag{16}$$

This condition is not satisfied in usual liquid crystals of rod-like molecules in which K_3 is larger than K_1 and K_2. By contrast, I will show in the experimental section that this condition can be fulfilled in liquid crystals containing flexible dimers such as CB7CB in which K_3 is anomalously small with respect to K_1 and K_2 [8–11]. Before that, I analyze the stability of the π-twisted solution.

B. Stability of the π-twisted solution

In practice, a π-twisted configuration develops in samples of thickness $|P_0|/4 < d < 3|P_0|/4$ [1]. It turns out that this solution is not always stable as I will show in the experimental section and develops a texture with a wave vector perpendicular to the anchoring direction (i.e., parallel to the director in midplane of the sample). For this reason, it becomes pertinent to analyze the stability of the π-twisted solution with respect to a perturbation of the type $\vec{n} = \vec{n}_0/\|\overrightarrow{n_0}\|$ with

$$\vec{n}_0 = \begin{pmatrix} \cos\left(\frac{\pi z}{d}\right) + \delta n_x \sin\left(\frac{\pi z}{d}\right)\sin(qy) \\ \text{sign}(q_0)\sin\left(\frac{\pi z}{d}\right) \\ \delta n_z \sin\left(\frac{\pi z}{d}\right)\sin(qy+\phi) \end{pmatrix}. \tag{17}$$

As before, the anchoring direction is along the x axis and the z axis is perpendicular to the plates. In this formula, $\text{sign}(q_0) = +1$ for a right-handed cholesteric and $\text{sign}(q_0) = -1$ for a left-handed cholesteric. The procedure is exactly the same as before. Calculating the average free energy leads to

$$F = \frac{K_2(\pi - dq_0)^2}{2d} + a\,\delta n_x^2 + b\,\delta n_z^2 + c\,\delta n_x \delta n_z, \tag{18}$$

where

$$\begin{cases} a = \frac{\pi^2 K_2}{8d} + \frac{1}{64}(K_1 + 5K_3)dq^2 \\ b = \frac{4\pi^2(K_1 - 2K_2 + K_3) + (K_2 + 3K_3)d^2q^2 + \text{sign}(q_0)8\pi K_2 dq_0}{32d} \\ c = -\frac{(\pi K_1 - 4\pi K_2 + 3\pi K_3 + \text{sign}(q_0)6K_2 dq_0)q\sin\phi}{16} \end{cases}. \tag{19}$$

The π-twisted configuration becomes unstable when the discriminant $\Delta = 4ab - c^2$ of this quadratic form becomes negative. This happens when $\phi = \pm\pi/2$ and when the ratio P_0/d is smaller (in absolute value) than

$$\left(\frac{P_0}{d}\right)_{\text{max2}} = \frac{36K_2}{\overline{K} + \sqrt{K\overline{K}^\star}}, \tag{20}$$

where

$$\begin{cases} K = K_1 + 5K_3 \\ K^\star = K_2 + 3K_3 \\ \overline{K} = -2K_1 + 12K_2 - 4K_3 + 6\sqrt{K_2K^\star} \\ \overline{K}^\star = 13K_1 - 12K_2 + 5K_3 + 12\sqrt{K_2K^\star} \end{cases}. \tag{21}$$

When $|P_0|/d = (P_0/d)_{\text{max2}}$, the discriminant vanishes for

$$|q| = q_{c2} = \frac{2\pi}{\sqrt{3}d}\sqrt{\frac{(K + \sqrt{K\overline{K}^\star})\sqrt{K_2}}{K\sqrt{K^\star}}}, \tag{22}$$

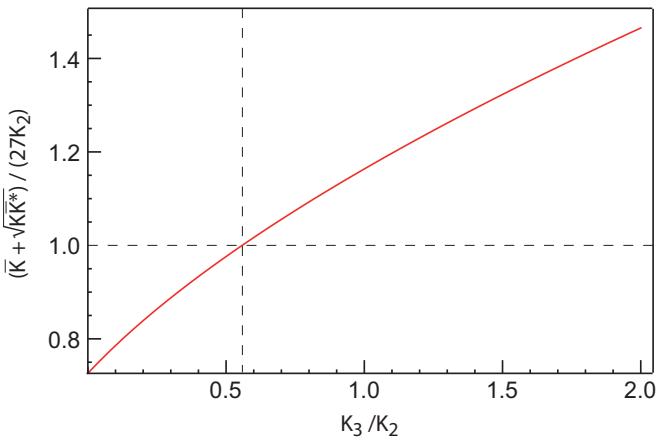

FIG. 1. Ratio $(\overline{K} + \sqrt{K\overline{K}^\star})/(27K_2)$ as a function of K_3/K_2 when $K_1 = K_2$.

which defines the wavelength at the onset of instability:

$$\lambda_{c2} = 2\pi/q_{c2} = \sqrt{3}d\sqrt{\frac{K\sqrt{K^\star}}{(K + \sqrt{K\overline{K}^\star})\sqrt{K_2}}}. \tag{23}$$

In practice this instability will be observable if $|P_0|/d > 4/3$—otherwise the π-twisted configuration is replaced by a 2π-twisted configuration, more favorable energetically—which imposes that

$$g_2(K_1, K_2, K_3) := \frac{\overline{K} + \sqrt{K\overline{K}^\star}}{27K_2} < 1. \tag{24}$$

In Fig. 1, I plotted this ratio as a function of K_3/K_2 by assuming that $K_1 = K_2$. It appears that this ratio is smaller than 1 when K_3 is small, less than $0.558K_2$. In usual liquid crystals, K_3 is larger than K_2, which explains why this instability is never observed. By contrast, K_3 is anomalously small in LC of flexible dimers such as CB7CB, making them good candidates for the observation of this instability. This is indeed the case as I will show in the next section.

Finally the ratio $\delta n_x/\delta n_z$ can be calculated by taking $\phi = \pi/2$ and $q = q_{c2}$. The calculation gives:

$$\frac{\delta n_x}{\delta n_z} = \text{sign}(q_0)\sqrt{\frac{1 + \sqrt{\overline{K}^\star/K}}{3}}\left(\frac{K^\star}{K_2}\right)^{1/4}. \tag{25}$$

In the limit $K_3 \ll K_1$ and K_2, one calculates $\delta n_x/\delta n_z \approx 1.24\,\text{sign}(q_0)$, which means that the director rotates on a cone slightly flattened in the center of the sample. We are thus again dealing with a heliconical instability.

III. EXPERIMENTAL EVIDENCE OF THE HELICONICAL INSTABILITIES

A. Materials and experimental setup

All my experiments were performed with a mixture of CB7CB and 8CB in equal proportion by weight doped with 0.182 wt% of the chiral molecule R811. This mixture has a cholesteric phase (Ch) between 30 and 61 °C and a twist-bend nematic (N_{TB}) phase below 30 °C. The two LCs, CB7CB, and

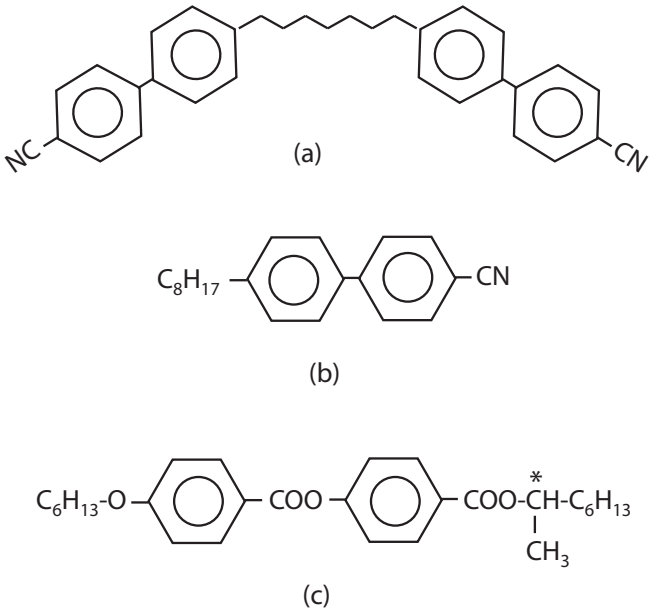

FIG. 2. Molecules used: (a) 1″, 7″-bis(4-cyanobiphenyl-4′–yl)heptane, CB7CB (flexible bend core); (b) 4-*n*-octylcyanobiphenyl, 8CB (rod-shaped); (d) R-(+)-octan-2-yl 4-((4-(hexyloxy)benzoyl)oxy) benzoate, R811 (chiral dopant).

8CB, were purchased at Synthon (Germany) and used without further purification. The molecule R811 was produced by Merck KGaA (Germany) and is known to give right-handed cholesteric phase in usual LCs. These molecules are shown in Fig. 2. The constants K_1 and K_3 were measured previously in the mixture CB7CB+50 wt% 8CB [11]. In addition, I measured K_2. The details on this measurement are given in Appendix A. Their variation in temperature is shown in Fig. 3. This figure shows that K_1 and K_2 increase when the temperature decreases whereas K_3 decreases and then increases when the temperature decreases. This increase of K_3 is generally attributed to the presence of the nematic twist-bend (N_{TB}) phase in which the molecules form pseudolayers [8,10]. I

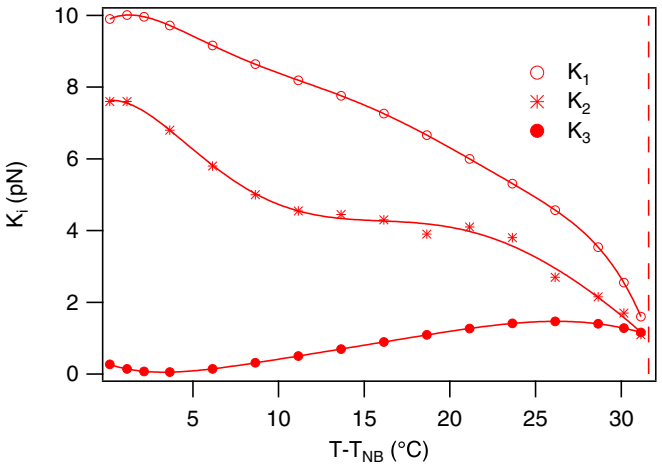

FIG. 3. Elastic constants as a function of temperature. The data for K_1 and K_3 are taken from Ref. [11]. The solid lines are the best fits with a polynomial of order 8.

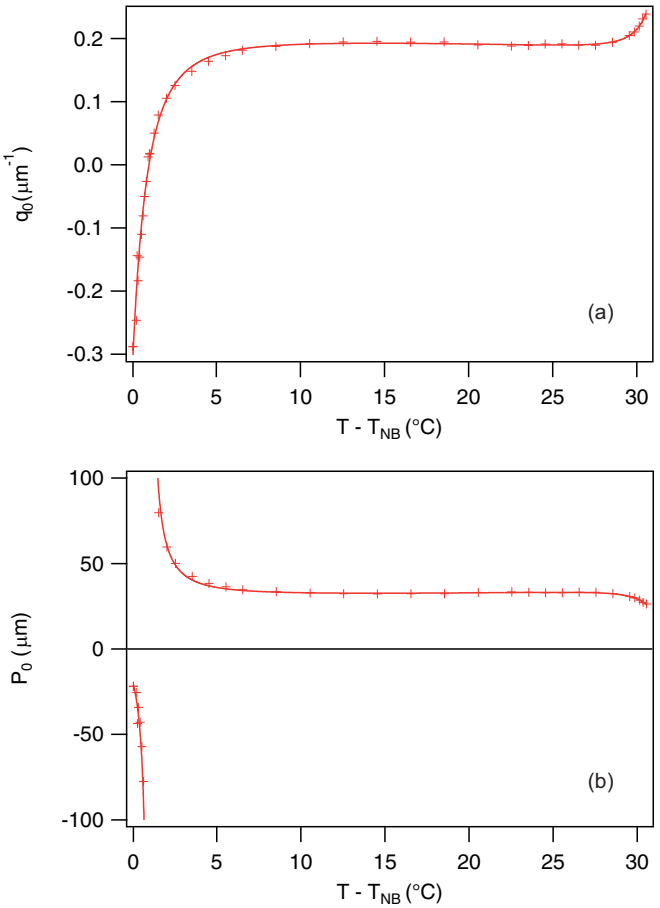

FIG. 4. (a) Equilibrium twist as a function of temperature. The solid line is the best fit with a function of the type $a + bx^2 + c/(x - x_0)^n + d(x_1 - x)^m$. (b) Equilibrium pitch as a function of temperature.

nonetheless note that neither K_3 nor K_2 seem to diverge at the N_{TB} phase transition, contrary to what is observed at the smectic A phase transition (when it is second order [1,11]). In the following, I will assume that the elastic constants are the same in my cholesteric mixture. This assumption is reasonable in view of the very small amount of R811 added in the mixture.

Another important parameter in my study is the temperature evolution of the equilibrium twist q_0. The classical method to measure q_0 is to use a Cano wedge [1]. It turns out that this method is not applicable here because of the heliconical instabilities that develop in the sample near the χ-disclination lines of the Cano wedge. Because of these instabilities, the lines no longer lie at places where $d = P_0/4, 3P_0/4, 5P_0/4, \ldots$ but shift towards smaller thicknesses, which makes this method inapplicable. In addition, the LC is very viscous, which constitutes another severe limitation to the use of a Cano wedge. For these reasons, I chose another method consisting in measuring the rotatory power of a thin sample sandwiched between a plate treated for planar unidirectional anchoring and a second one treated for planar sliding anchoring. The details of this measurement are reported in Appendix B. The temperature evolution of the equilibrium twist q_0 and of the pitch P_0 are shown in Fig. 4. As expected with *R*811, I found that the cholesteric is right

handed at high temperature ($q_0 > 0$). I also observed that q_0 decreases when the temperature decreases, which I expected upon approaching T_{NB} because of the layered structure of the N_{TB} phase. However, I observed that q_0 vanishes and changes sign in the cholesteric phase at a temperature T_c slightly larger than T_{NB} ($T_c - T_{NB} \approx 0.9\,^{\circ}$C). The presence of this compensation point is surprising. This behavior contrasts with that previously observed in similar mixtures doped with larger concentrations of chiral molecules in which the pitch seems to diverge at T_{NB} [12]. It turns out that this unexpected property is very interesting to test the present theory on the heliconical instability induced by confinement.

All observations were made with a Leica Laborlux 12 Pol Microscope equipped with a Guppy F-503 CMOS camera. The samples were prepared between indium tin oxide (ITO) coated glass slides. Their thickness was fixed thanks to nickel wires used as a spacer and was measured with an Ocean Optics USB2000 spectrometer. A homemade oven was used to fix the temperature of the samples. The temperature was regulated to within $\pm 0.01^{\circ}$C thanks to an ATNE ATSR100 PID temperature controller. The polyimide Nissan 0825 was used to prepare the plates treated for planar unidirectional anchoring according to the protocol described in Ref. [11]. A thin polymercaptan layer was used to obtain a planar sliding anchoring according to the protocol described in Ref. [13].

B. About the choice of the current cholesteric mixture

The theory predicts that the heliconical instability may develop in the unwound configuration if condition (16) is satisfied and in the π-twisted configuration if condition (24) is satisfied. To test these predictions, I plotted the functions $g_1(K_1, K_2, K_3)$ and $g_2(K_1, K_2, K_3)$ given in Eqs. (16) and (24) as a function of temperature in Fig. 5. These functions were calculated by using the polynomial fits of the elastic constants shown in Fig. 3. These two graphs show that the two functions are less than 1 in a large interval of temperature above T_{NB}, making the mixture CB7CB+50 wt% 8CB a good candidate to evidence the heliconical instability in confined geometry.

C. Experimental evidence of the heliconical instability in an unwound sample

To observe the instability in the unwound cholesteric, the sample thickness must be adequately chosen. Indeed, this instability will develop if the cholesteric pitch P_0 satisfies $4 < |P_0|/d < (P_0/d)_{max1}$. A good choice of thickness is $d = 7.5\,\mu$m as can be seen in Fig. 6(a) in which I plot the ratio $|P_0|/d$ measured experimentally and the two limits $P_0/d = 4$ and $P_0/d = (P_0/d)_{max1}$ given by Eq. (10). This graph shows that the instability must develop in two intervals of temperature: very close to the transition to the N_{TB} phase between T_{NB} and T_1 (with $T_1 - T_{NB} \approx 0.65\,^{\circ}$C) and between T_2 and T_3 (with $T_2 - T_{NB} \approx 1.44\,^{\circ}$C and $T_3 - T_{NB} \approx 13.2\,^{\circ}$C). At these temperatures, the wavelength of the instability can be calculated by using the graph of Fig. 6(b) in which λ_{c1}/d has been plotted by using Eq. (12) and the polynomial fits of the elastic constants shown in Fig. 2. This gives $\lambda_{c1}(T_1) \approx 2.25\,\mu$m, $\lambda_{c1}(T_2) \approx 1.75\,\mu$m and $\lambda_{c1}(T_3) \approx 5.05\,\mu$m.

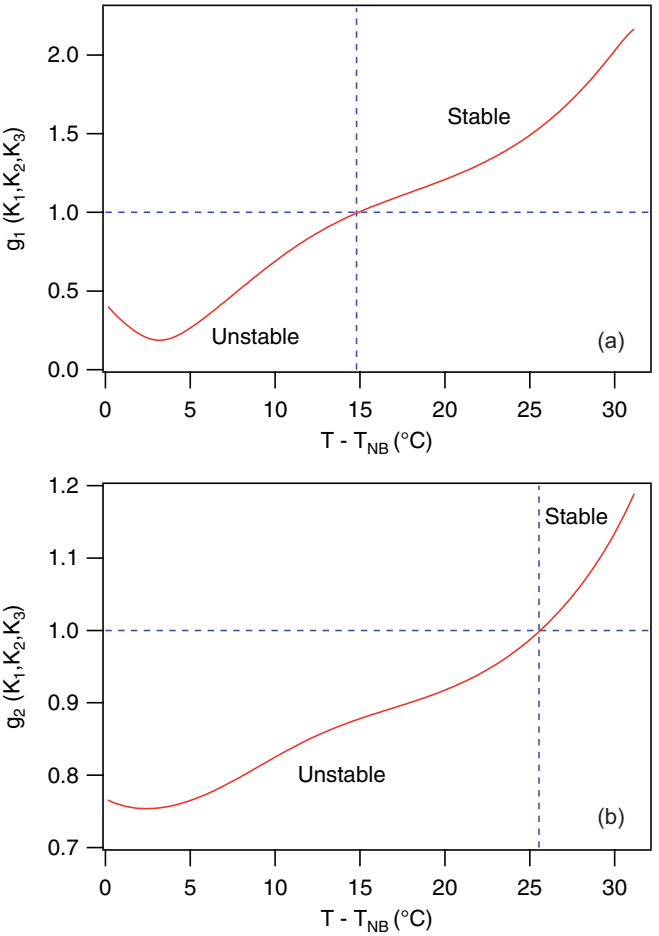

FIG. 5. Functions (a) g_1 and (b) g_2 as a function of temperature calculated for the mixture CB7CB+50 wt% 8CB by using the polynomial fits of the elastic constants shown in Fig. 3.

To test these theoretical predictions, I prepared a 7.5 μm-thick sample of the cholesteric mixture and I observed it under the microscope. All the observations were made with the polarizer and the analyzer parallel to the anchoring direction on the plates. As expected, I observed that the cholesteric phase was unwound and stable at high temperature. On the other hand, I observed, by decreasing the temperature, that a band texture—with the bands perpendicular to the anchoring direction—successively developed in two intervals of temperature, between $T_3(\text{exp}) \approx 42\,^{\circ}$C and $T_2(\text{exp}) \approx 34\,^{\circ}$C and then between $T_1(\text{exp}) \approx 30.5\,^{\circ}$C and $T_{NB} \approx 30\,^{\circ}$C. Outside of these two intervals, the bands disappear, as predicted theoretically in the previous section. A few micrographs of the band texture are shown in Fig. 7 and the wavelengths measured experimentally are shown in Fig. 8. Note that before each measurement of the wavelength, the sample was equilibrated during half an hour typically. The equilibration was possible thanks to the climb of the numerous edge dislocations present in the band texture. Some of them are visible in Fig. 7(c), for instance. In Fig. 8 the three wavelengths λ_{c1} calculated theoretically at the onset of the heliconical instability (filled symbols in the graph) are also reported. The curves $\lambda_{min}(T)$ and $\lambda_{max}(T)$ calculated from Eqs. (14) by using the fits of the elastic constants and of the equilibrium twist are also

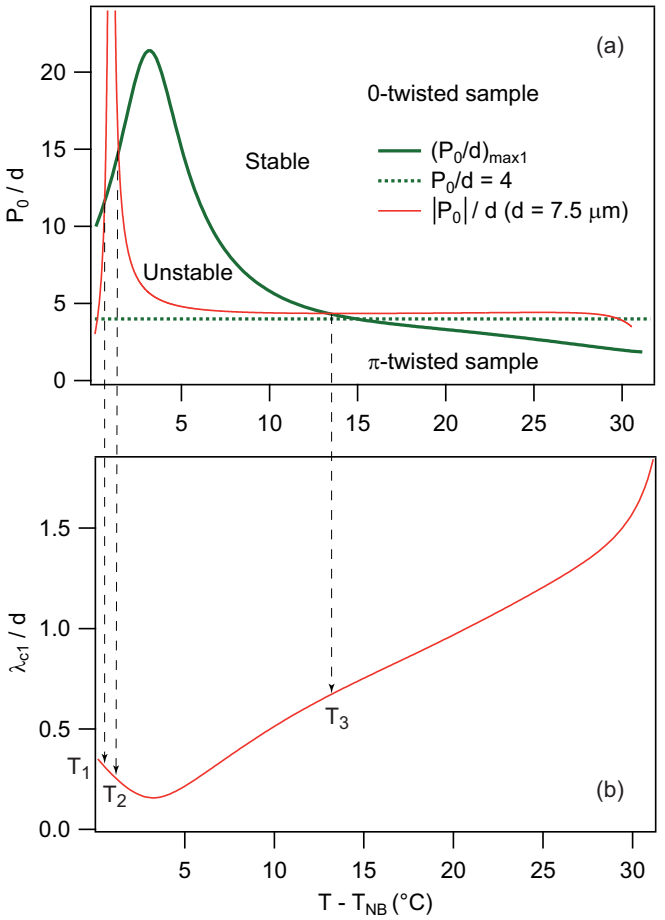

FIG. 6. Graphical determination of the temperatures T_1, T_2, and T_3 (indicated by the three vertical arrows) at which the instability occurs and of the corresponding wavelengths. In (a) I plot as a function of temperature the curve $(P_0/d)_{max1}$, the curve $P_0/d = 4$ marking the limit between the unwound and the π-twisted configurations and the experimental curve $|P_0|/d$ ($d = 7.5\,\mu$m) and in (b) the curve λ_{c1}/d is plotted.

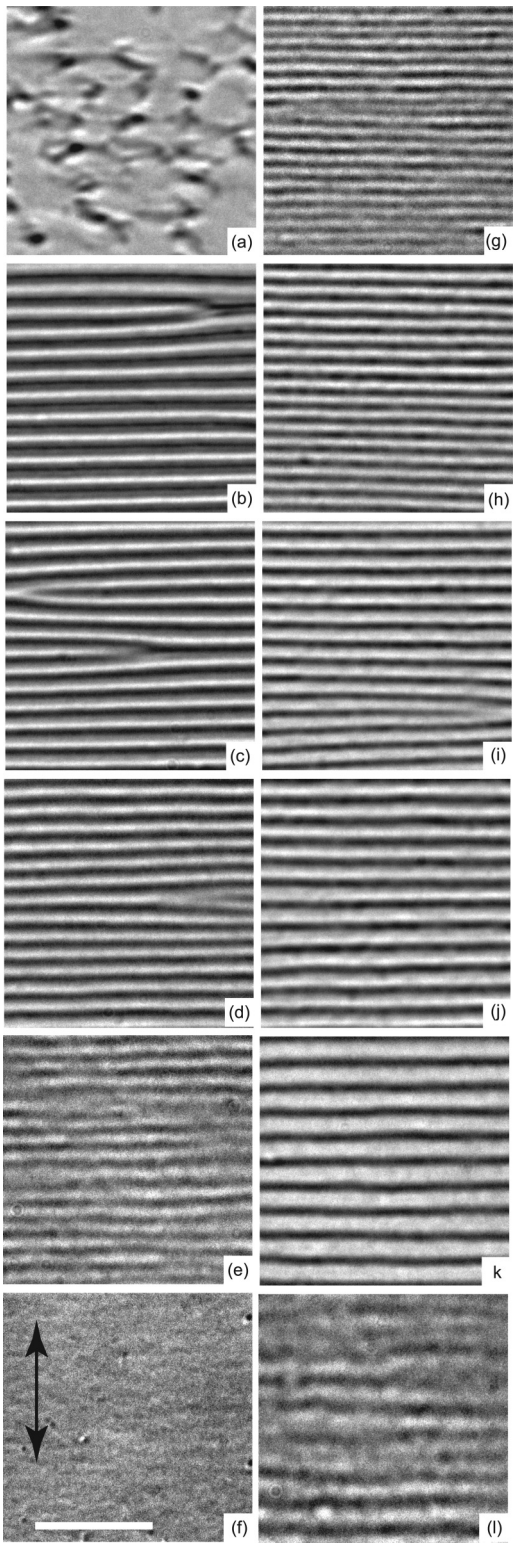

FIG. 7. Snapshots of the band texture observed in a 7.5 μm-thick sample as a function of temperature. The vertical double arrow indicates the rubbing direction and the white bar is 20 μm long. From (a) to (l), $T = 29.95$ (N_{TB} phase), 30.1, 30.2, 30.3, 30.35, 30.5, 31.3, 32.5, 33.5, 35, 37, 39, 41 °C.

plotted (dashed and solid lines, respectively). This graph shows that there is a good quantitative agreement between the theoretical predictions and the experiment. In particular, the measured wavelengths extrapolate well to wavelengths λ_{c1} theoretically calculated at temperatures T_1, T_2, and T_3. Note that the temperatures T_1, T_2, and T_3 measured experimentally are a bit different from the predicted temperatures. This is normal because the band contrast strongly decreases when the bifurcation (presumably of the second order) is approached, making the bands difficult to discern under the microscope at the onset of instability.

In practice, it should always be possible to observe the heliconical instability of the unwound configuration in the vicinity of the compensation point, because the pitch diverges at this temperature (see Fig. 6). To check this point, I prepared two samples of thickness $d = 14.5\,\mu$m and $d = 26\,\mu$m, which I unwound at temperature $T_c \approx 30.9\,^\circ$C. In agreement with the theory, I observed that the texture was stable within a narrow interval of temperature $[T_1(\text{exp}]), T_2(\text{exp})]$ around T_c and destabilized by forming bands perpendicular to the anchoring direction outside of this interval. The band wavelength as a function of temperature is shown in Fig. 8 for the two samples and compared to the wavelengths $\lambda_{c1}(T_1)$

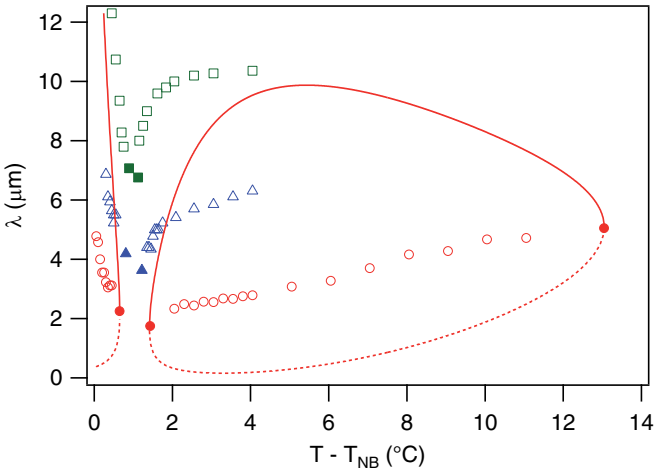

FIG. 8. Wavelength of the band texture observed in an unwound sample as a function of temperature. The open symbols represent the experimental points and the filled symbols represent the theoretical predictions at the onset of the heliconical instability (λ_{c1}). For the red circles $d = 7.5\ \mu$m, for the blue triangles $d = 14.7\ \mu$m and for the green squares $d = 26\ \mu$m. The red solid (dashed) line corresponds to $\lambda_{\max}$ ($\lambda_{\min}$) calculated for $d = 7.5\ \mu$m by using Eqs. (14). All the wavelengths inside the domain bounded by these two curves are unstable. The measured wavelengths are well inside this domain. For more clarity, the curves $\lambda_{\max}$ and $\lambda_{\min}$ are not plotted for the two other thicknesses.

and $\lambda_{c1}(T_2)$ predicted by the theoretical model. Again, the agreement between theory and experiment is good.

D. Experimental evidence of the heliconical instability in a π-twisted sample

As previously, the sample thickness must be adequately chosen to observe the heliconical instability in a π-twisted configuration. Indeed, the cholesteric pitch must now satisfy conditions $4/3 < |P_0|/d < 4$ and $|P_0|/d < (P_0/d)_{\max 2}$. This is the case for a sample of thickness $d = 22.7\ \mu$m as can be seen in Fig. 9. According to this figure (identical to Fig. 6), a heliconical instability should appear in the π-twisted configuration only in the temperature interval $[T_4, T_5]$ with $T_4 - T_{NB} \approx 3.6\,^{\circ}$C and $T_5 - T_{NB} \approx 20.7\,^{\circ}$C. At these temperatures the theory predicts that $\lambda_{c2}(T_4) \approx 19.5\ \mu$m and $\lambda_{c2}(T_4) \approx 23.4\ \mu$m.

To test these predictions, I made a 22.7 μm-thick sample of the cholesteric mixture and I observed its texture under the microscope. All the observations were made with the polarizer and the analyzer parallel to the anchoring direction on the plates. As predicted, I observed that the sample was twisted by π and stable at high temperature (except very close to the clearing temperature where 2π-twisted domains nucleated due of the decreasing of the pitch, see Fig. 4). Subsequently, I observed by decreasing the temperature that a band texture formed between $T_5(\text{exp}) \approx 50\,^{\circ}$C and $T_4(\text{exp}) \approx 35\,^{\circ}$C. A few snapshots of this texture are shown in Fig. 10 and the wavelengths measured experimentally after a recovery of about half an hour are shown in Fig. 11. The two wavelengths $\lambda_{c2}(T_4)$ and $\lambda_{c2}(T_5)$ are also given in this graph. Again the agreement between the theory and the experiment is satisfactory.

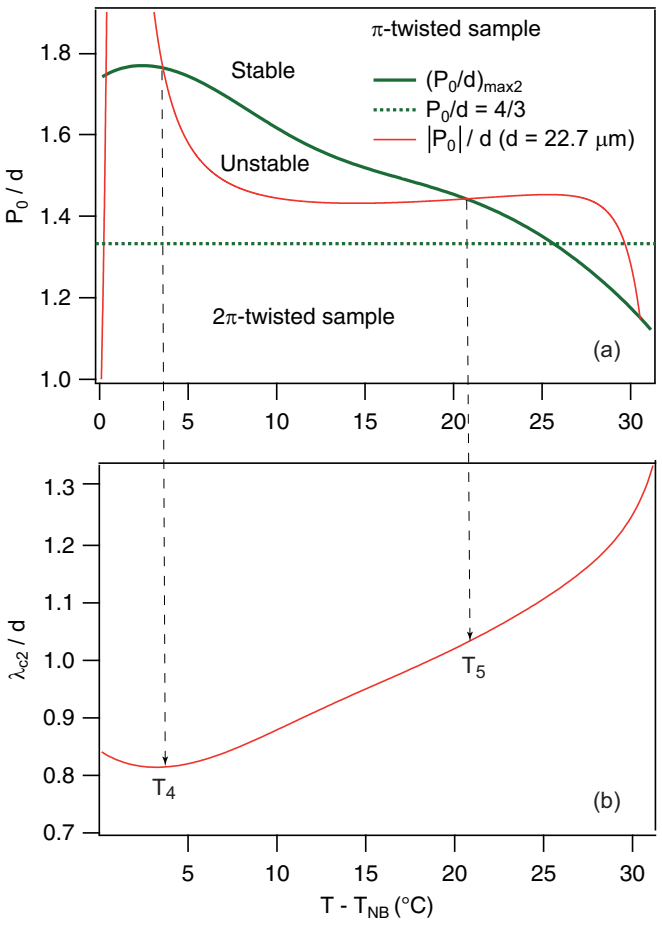

FIG. 9. Graphical determination of the temperatures T_4 and T_5 (indicated by the two vertical arrows) at which the instability occurs and of the corresponding wavelengths. In (a) are plotted as a function of temperature the curve $(P_0/d)_{\max 2}$, the curve $P_0/d = 4/3$ marking the limit between the π and the 2π-twisted configurations and the experimental curve $|P_0|/d$ (with $d = 22.7\ \mu$m) and in (b) is plotted the curve λ_{c2}/d.

IV. CONCLUSION AND PERSPECTIVES

By doping with a small concentration of chiral molecules the mixture CB7CB+50 wt% 8CB in which K_3 is anomalously small, I was able to evidence the heliconical instability predicted by Poy and Žumer in a cholesteric confined between two plates treated for strong planar anchoring [7]. I found that this instability could develop not only in the unwound state (as predicted by these authors) but also in the π-twisted state in which I generalized the calculation of stability. In the two cases, I found a good agreement between the theory and the experiment, and this without any adjustable parameters. In particular, the intervals of temperature in which the instability develops are correctly predicted by the theory as well as the wavelengths at the onset of the instability.

A natural extension of this work would be to perform a nonlinear analysis of this instability to prove it is second order as it seems to be the case experimentally. It would also be interesting to numerically compute the wavelength in the nonlinear regime to compare with the experimental values. These calculations could also be generalized to more twisted

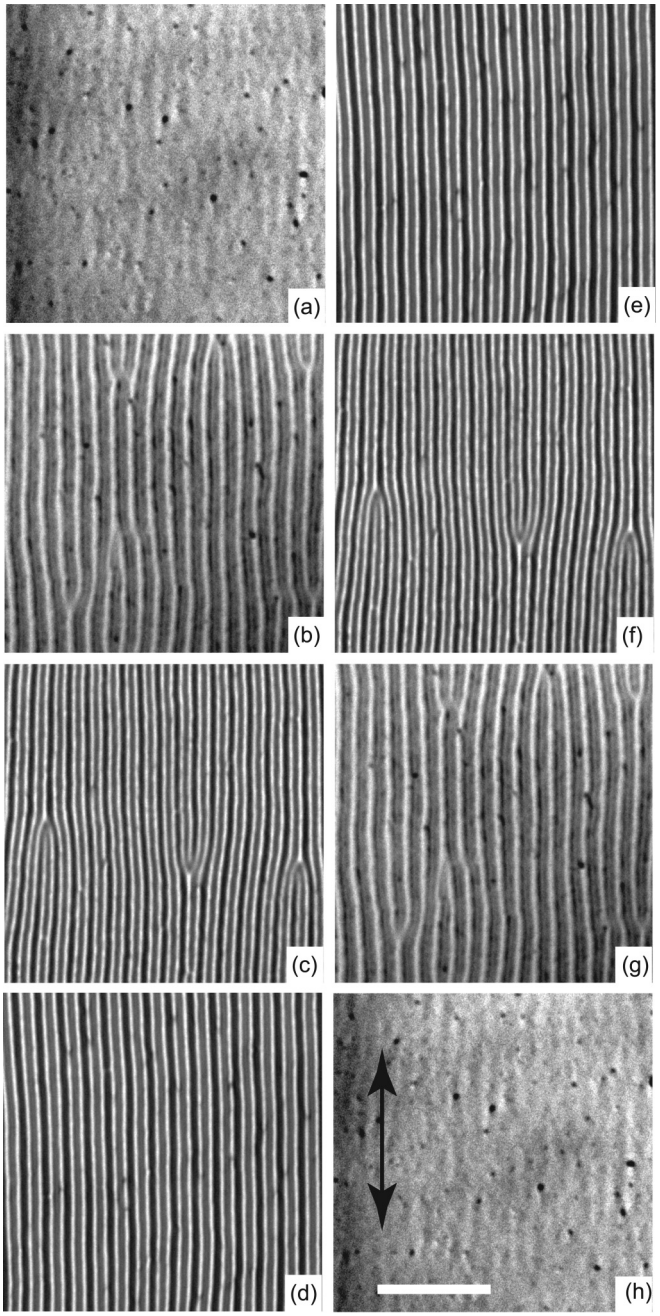

FIG. 10. Snapshots of the band texture observed in a 22.7 μm-thick sample as a function of temperature. The vertical double arrow indicates the rubbing direction and the white bar is 100 μm long. From (a) to (h), $T = 35, 36, 37, 41, 45, 47, 49, 50\,^{\circ}$C.

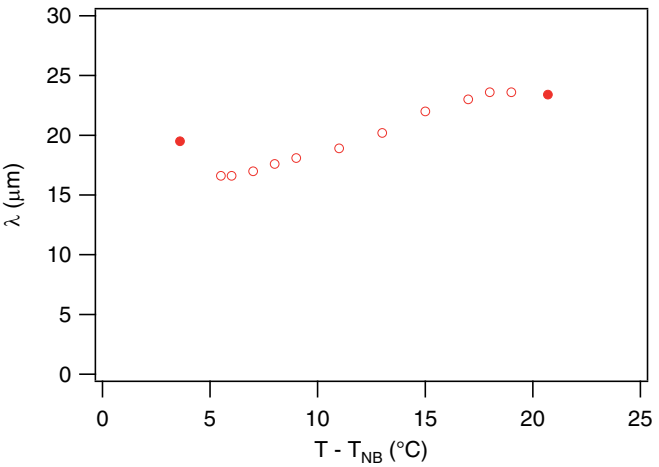

FIG. 11. Wavelength of the band texture observed in a π-twisted sample as a function of temperature. The open symbols represent the experimental points and the filled symbols represent the theoretical predictions at the onset of the heliconical instability. The cell spacing is $d = 22.7\ \mu$m.

configurations in which this instability still exists as I have found by making a Cano wedge. In particular, a similar band texture, with the bands perpendicular to anchoring direction develops in the 2π-twisted region near the third χ line separating the 2π- and 3π-twisted regions. I emphasize once again that the presence of this instability makes impossible a precise measurement of the pitch with the Cano wedge technique because the lines are no longer at positions $d = P_0/4, 3P_0/4, 5P_0/4, \ldots$ as it must be without instability.

A surprising point of this study is the existence of a compensation temperature in the mixture chosen. This observation is unusual for several reasons:

First, because a compensation point is not observed in ordinary liquid crystals doped with R811. However, such a behavior is usually observed with particular chiral molecules such as the esters of cholesteryl. In this category, the cholesteryl choride (CC) is the most popular [14].

Second, because this compensation point is observed at very low concentration of chiral molecules. This is again unusual as most of the liquid crystals have a compensation point at concentrations of chiral molecules close to 50%. This is the case in the mixtures of ordinary liquid crystals such as 8CB or MBBA (p-methyloxybenzilidene-*p*-n-butylaniline) doped with CC. Note nonetheless one exception in the mixture CCN37 (4α, $4'\alpha$-propylheptyl-1α, $1'\alpha$-bicyclohexyl-4β-carbonitrile) + CC in which a compensation point was observed for a concentration of CC close to 3% [15].

Third, because the pitch does not diverge at the phase transition towards the N_{TB} phase in spite of its lamellar-like structure [5]. This result is compatible with the absence of a clear divergence of the twist constant K_2 at T_{NB} as can be seen in Fig. 3 (the divergence of K_2 is indeed responsible for the divergence of the pitch at the cholesteric-smectic A phase transition [16]).

In the future, it would be interesting to test other chiral molecules to check if the presence of the compensation point is due to R811 or to a particular property of the mixture CB7CB/8CB such as the proximity of a N_{TB} phase. Another interesting point would be to change the concentration of R811 to see if the compensation point disappears. This should be the case if I refer to a recent work by Kasian *et al.* [12] in which there is no mention of a compensation point in similar mixtures doped with a larger concentration of R811 (more than 4% in their paper).

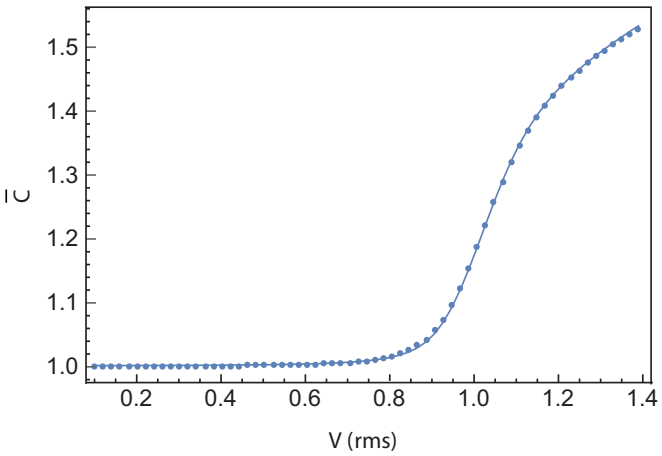

FIG. 12. Capacitance curve measured at $T = 40\,^{\circ}\mathrm{C}$. The critical voltage V_c is not well defined. The solid line is the best fit with the theoretical curve calculated by taking into account the pretilt angle on the plates.

ACKNOWLEDGMENTS

The authors warmly thank J. Ignès-Mullol and G. Poy for their critical reading of the manuscript and useful comments and Dr. W. Becker from Merck for the sample of R811.

APPENDIX A: EXPERIMENTAL MEASUREMENT OF K_2

A classical method to determine K_2 is to measure the critical Fredericksz voltage in a planar sample twisted by $\pi/2$. If the anchoring is strong and if there is no pretilt angle, the critical voltage is given by

$$V_c = \pi\sqrt{\frac{K_1 + \frac{K_3 - 2K_2}{4}}{\varepsilon_0 \varepsilon_a}}, \tag{A1}$$

where ε_0 is the vacuum permittivity and $\varepsilon_a = \varepsilon_\parallel - \varepsilon_\perp$ is the dielectric anisotropy. Thus, measuring V_c allows us in principle to measure K_2 provided that ε_a and the elastic constants K_1 and K_3 are known. This is the case for the mixture CB7CB + 50 wt% 8CB in which these constants have already been measured [11].

To implement this method, I prepared a twisted sample of thickness $d = 50\ \mu$m. Each ITO electrode was treated for planar unidirectional anchoring with the polyimide Nissan 0825 by following the same protocol as in Ref. [11]. A RLC meter HP 4284A was used to measure the sample capacitance as a function of the applied voltage. All measurements were performed at 50 kHz in the dielectric regime. A typical capacitance curve is shown in Fig. 12. This example shows that the capacitance curve is rounded at the onset of instability, making a direct determination of V_c very imprecise, if not impossible. This problem is due to the presence of a small pretilt angle θ_a at the surface of the electrodes.

To take into account this angle, I solved numerically with *Mathematica* the full set of equations given the capacitance as a function of the applied voltage. To simplify, I assumed that the anchoring energy was infinite, which is a good approximation at large thickness as in my experiment. The equations to solve read [17]:

$$\begin{cases} \dfrac{d}{2} = \displaystyle\int_{\theta_a}^{\theta_m} f_1(\theta, \theta_m, \phi_m', \overline{C})d\theta \\ \dfrac{\pi}{2} = \displaystyle\int_{\theta_a}^{\theta_m} f_2(\theta, \theta_m, \phi_m', \overline{C})d\theta \\ \dfrac{V}{2} = \dfrac{D}{\varepsilon_0 \varepsilon_\parallel}\displaystyle\int_{\theta_a}^{\theta_m} f_3(\theta, \theta_m, \phi_m', \overline{C})d\theta. \end{cases} \tag{A2}$$

The first two come from the bulk torque equation and the third one comes from the Maxwell equation for the electric field. In these equations, $\overline{C} = C/C_\perp$ is the capacitance normalized with the capacitance $C_\perp = \frac{\varepsilon_0 \varepsilon_\perp S}{d}$ (with S the electrode surface area) and

$$\begin{cases} f_1(\theta, \dots) = \sqrt{\dfrac{1 - \gamma_1 \sin^2\theta}{(\cos^2\theta - \cos^2\theta_m)g(\theta, \dots)}} \\ f_2(\theta, \dots) = \dfrac{\cos^2\theta_m(1 - \gamma_2\cos^2\theta_m)}{\cos^2\theta(1 - \gamma_2\cos^2\theta)} f_1(\theta, \dots), \\ f_3(\theta, \dots) = \dfrac{1}{1 - \alpha\cos^2\theta} f_1(\theta, \dots) \end{cases} \tag{A3}$$

where

$$\begin{aligned} &g(\theta, \theta_m, \phi_m', \overline{C}) \\ &= D^2 \frac{\alpha}{K_3 \varepsilon_0 \varepsilon_\parallel} \frac{1}{(1 - \alpha\cos^2\theta)(1 - \alpha\cos^2\theta_m)} \\ &+ \frac{\cos^2\theta_m(1 - \gamma_2\cos^2\theta_m)(1 - \gamma_2(\cos^2\theta + \cos^2\theta_m))}{\cos^2\theta(1 - \gamma_2\cos^2\theta)} \phi_m'^{\,2}. \end{aligned} \tag{A4}$$

Angles θ and ϕ are the polar and azimuthal angles, with $\theta = \theta_a$ and $\phi = 0$ on the bottom electrode at $z = 0$ and $\theta = \theta_a$ and $\phi = \pi/2$ on the top electrode at $z = d$, $\theta_m = \theta(d/2)$, $\phi_m' = (d\phi/dz)(d/2)$, $\gamma_1 = 1 - K_1/K_3$, $\gamma_2 = 1 - K_2/K_3$, $\alpha = \varepsilon_a/\varepsilon_\parallel$, and $D = CV/S = \varepsilon_0\varepsilon_\perp(V/d)\overline{C}$ is the electric displacement, constant within the sample thickness in the dielectric regime.

To solve the set of equations (A2) with unknowns θ_m, ϕ_m', and $\overline{C}$, I used the values of K_1, K_3, and ε_a given in Ref. [11] and I fitted the capacitance curves by taking θ_a and K_2 as fit parameters. The best fits—one example is shown in Fig. 12—were obtained for $\theta_a = 1.8^\circ$, which is a little bit larger than the value of 1.7° given in Ref. [11]. The values of K_2 obtained in this way are shown in Fig. 3.

APPENDIX B: EXPERIMENTAL MEASUREMENT OF P_0

It turns out that the Cano wedge method is not suitable to measure the pitch of the current cholesteric mixture. The main reason is the presence of the heliconical instability, which develops at low temperature in the vicinity of the χ lines. Another problem comes from the large viscosity of the phase, in particular close to the N_{TB} phase, which considerably increases the equilibration time of the samples. For these two reasons, I have chosen another more versatile method consisting of measuring the rotatory power of the cholesteric phase. To this end, I made two 8 μm-thick cells, each of them with the bottom plate treated for planar unidirectional

anchoring with the polyimide Nissan 0825 while the top plate was treated for planar sliding anchoring with a polymercaptan layer, following the protocols given in Refs. [11] and [13].

The first cell was filled with the nematic mixture CB7CB+50 wt% 8CB. With this cell, I measured the birefringence of the liquid crystal by using a Berek rotating compensator Leica 0989. A red filter ($\lambda = 633$ nm) was used. With this sample, I found that the apparent birefringence was the same (to within 5%) as the one found previously with a planar parallel sample [11]. This proves that the anchoring is well planar at the interface with the polymercaptan.

The second cell was filled with the cholesteric mixture and illuminated with a polarized light beam whose incident polarization was parallel to the director on the bottom plate. I then measured with the CCD camera the transmitted intensity I_{tr} in red light ($\lambda = 633$ nm) across the rotating analyzer of the microscope and I determined for which angle $\phi_{\max}$ of angle ϕ between the polarizer and the analyzer I_{tr} was maximum. From this measurement, I deduced the rotation angle θ of the director across the sample thickness. The pitch was then calculated by using the formula $P_0 = 2\pi d/\theta$. The results are shown in Fig. 4.

Note that when the birefringence is large (rigorously when $P_0\Delta n \gg \lambda$) there is adiabatic rotation of the light polarization, so that one has simply $\theta = \phi_{\max}$. In my experiment, this condition was not always fulfilled, in particular close to the melting temperature where Δn decreases. For this reason, I systematically used the Ong formula [18,19]

$$I_{tr}(\phi) = \cos^2(\theta - \phi) - \frac{\cos[2(\theta-\phi)]\sin^2[\theta\sqrt{1+u^2}]}{1+u^2} + \frac{\sin[2(\theta-\phi)]\sin[2\theta\sqrt{1+u^2}]}{2\sqrt{1+u^2}} \tag{B1}$$

in which $u = \frac{\pi d\Delta n}{\theta\lambda}$ to calculate with *Mathematica* the correct value of θ corresponding to $\phi_{\max}$.

Last but not least, I mention that my measurements were performed by both decreasing and increasing the temperature. In doing this, no hysteresis was observed, meaning that the anchoring was perfectly sliding during the measurements. The same behavior was incidentally observed during several days with the same sample, without notable memorization of an anchoring direction, even when the temperature was kept constant. This behavior is different from the one observed with pure cyanobiphenyls in which memorization effects occur after a few hours [20]. This behavior is clearly due to the presence of CB7CB and could be interesting for applications that require a sliding anchoring.

[1] P. Oswald and P. Pieranski, *Nematic and Cholesteric Liquid Crystals: Concepts and Physical Properties Illustrated by Experiments* (Taylor & Francis, CRC Press, Boca Raton, 2005).

[2] R. B. Meyer, Effects of electric and magnetic fields on the structure of cholesteric liquid crystals, Appl. Phys. Lett. **12**, 281 (1968).

[3] P. G. de Gennes, Calcul de la distorsion d'une structure cholesterique par un champ magnetique, Solid State Commun. **6**, 163 (1968).

[4] J. Xiang, S. V. Shiyanovskii, C. Imrie, and O. D. Lavrentovich, Electrooptic Response of Chiral Nematic Liquid Crystals with Oblique Helicoidal Director, Phys. Rev. Lett. **112**, 217801 (2014).

[5] A. Jákli, O. D. Lavrentovich, and J. V. Selinger, Physics of liquid crystals of bent-shaped molecules, Rev. Mod. Phys. **90**, 045004 (2018).

[6] O. D. Lavrentovich, Electromagnetically tunable cholesterics with oblique helicoidal structure, Opt. Mat. Express **10**, 2415 (2020).

[7] G. Poy and S. Žumer, Chirality-enhanced nonlinear optical response of frustrated liquid crystals, in *Liquid Crystals XXV*, Vol. 11807 (International Society for Optics and Photonics, Bellingham, 2021), p. 1180708.

[8] G. Babakhanova, Z. Parsouzi, S. Paladugu, H. Wang, Yu A. Nastishin, S. V. Shiyanovskii, S. Sprunt, and O. D. Lavrentovich, Elastic and viscous properties of the nematic dimer CB7CB, Phys. Rev. E **96**, 062704 (2017).

[9] O. S. Iadlovska, G. Babakhanova, G. H. Mehl, C. Welch, E. Cruickshank, G. J. Strachan, J. M. D. Storey, C. T. Imrie, S. V. Shiyanovskii, and O. D. Lavrentovich, Temperature dependence of bend elastic constant in oblique helicoidal cholesterics, Phys. Rev. Research **2**, 013248 (2020).

[10] A. Aouini, M. Nobili, E. Chauveau, P. Dieudonne-George, G. Dameme, D. Stoenescu, I. Dozov, and C. Blanc, Chemical-physical characterization of a binary mixture of a twist bend nematic liquid crystal with a smectogen, Crystals **10**, 1110 (2020).

[11] P. Oswald and J. Colombier, On the measurement of the bend elastic constant in nematic liquid crystals close to the nematic-to-SmA and the nematic-to-N_{TB} phase transitions, Liq. Cryst. (2021), doi: 10.1080/02678292.2021.1896041.

[12] N. A. Kasian, L. N. Lisetski, and I. A. Gvozdovskyy, Twist-bend nematics and heliconical cholesterics: a physico-chemical analysis of phase transitions and related specific properties, Liq. Cryst. (2021), doi: 10.1080/02678292.2021.1970838.

[13] P. Oswald, A. Dequidt, and A. Żywociński, Sliding planar anchoring and viscous surface torque in a cholesteric liquid crystal, Phys. Rev. E **77**, 061703 (2008).

[14] H. Hanson, A. J. Dekker, and F. Van der Woude, Analysis of the pitch in binary cholesteric liquid crystal mixtures, J. Chem. Phys. **62**, 1941 (1975).

[15] P. Oswald, G. Poy, and A. Dequidt, Lehmann rotation of twisted bipolar cholesteric droplets: role of Leslie, Akopyan and Zel'dovich thermomechanical coupling terms of nematodynamics, Liq. Cryst. **44**, 969 (2017).

[16] P. Oswald and P. Pieranski, *Smectic and Columnar Liquid Crystals: Concepts and Physical Properties Illustrated by Experiments* (Taylor & Francis, CRC Press, Boca Raton, 2006).

[17] H. A. Van Sprang and P. A. Breddels, Numerical calculations of director patterns in highly twisted nematic

configurations with nonzero pretilt angles, J. Appl. Phys. **60**, 968 (1986).

[18] H. L. Ong, Origin and characteristics of the optical properties of general twisted nematic liquid-crystal displays, J. Appl. Phys. **64**, 614 (1988).

[19] I.-C. Khoo and S.-T. Wu, *Optics and Nonlinear Optics of Liquid Crystals*, Vol. 1 (World Scientific, Singapore, 1993), p. 126.

[20] P. Oswald, Easy axis memorization with active control of the azimuthal anchoring energy in nematic liquid crystals, Europhys. Lett. **107**, 26003 (2014).